Engineering Journal issn: 0125-8281

Article

Optimization of Forming Process Parameters for Automotive Advanced High Strength Steel Parts Using the Taguchi Method

Aekkapon Sunanta[1], Weerapong Julsri[2], and Surasak Suranuntchai[1,*]

1 Department of Tool and materials Engineering, Faculty of Engineering, King Mongkut's University of Technology Thonburi, Bangkok, Thailand
2 Department of Industrial Engineering, Faculty of Industry and Technology, Rajamangala University of Technology Isan, Sakon Nakhon, Thailand
*E-mail: surasak.sur@kmutt.ac.th (Corresponding author)

Abstract. This paper presents a comparative analysis between finite element simulation results and actual formed parts, utilizing different material model combinations. The Bow-RF panel part made from JSC980Y advanced high strength steel was chosen as a case study and investigated by using the finite element method (FEM). The comparison revealed that the combination of the Barlat 1989 yield criterion and the Yoshida-Uemori hardening rule in the finite element simulation gave the best predicted result of the panel part during the drawing process. This combination achieved the highest percentage of area in the displacement range of -1 to 1 mm (approximately 83.17%). Subsequently, Taguchi's Design of Experiments (DOE) and Analysis of Variance (ANOVA) were employed to analyze the influence of each process parameter on the simulation results, including blank holder force, die gap, and blank width. Finally, a statistical mathematical model was created using regression analysis. The results indicated that the most influential parameters, in decreasing order of significance, were die gap, blank holder force, and blank width. The optimal process parameters for achieving the highest percentage of area in the displacement range within -1 to 1 mm were determined to be a blank holder force of 41.21 tons, a die gap of 0.9 mm, and a blank width of 297.47 mm.

Keywords: Advanced high strength steel, automotive part, finite element method, regression analysis, Taguchi.

ENGINEERING JOURNAL Volume 28 Issue 10
Received 3 April 2024
Accepted 30 September 2024
Published 31 October 2024
Online at https://engj.org/
DOI:10.4186/ej.2024.28.10.25

DOI:10.4186/ej.2024.28.10.25

1. Introduction

The automotive industry faces challenges in sheet metal forming such as reducing vehicle weight, meeting strict air quality regulations, and increasing passenger safety performance. These challenges leading to extensive research on alternative materials like high strength steel, carbon fiber composites, and various alloys [1]. Among these alternatives, advanced high strength steels (AHSS) have gained attention for their superior properties including high elongation and strength [2-3]. However, using AHSS in forming processes presents challenges including fracture, wrinkling, and springback [2]. Springback is the most significant problem in AHSS forming because it is a dimensional defect directly related to the workpiece size and can cause assembly issues. Springback refers to the tendency of the material to return to its original shape after bent or formed. This phenomenon occurs because the material retains an internal elastic memory that resists permanent deformation, even during plastic deformation, as some elastic regions attempt to return to their original shape. Engineers and researchers employ various methods to compensate for springback, such as adjusting tooling or using advanced simulation techniques to accurately predict the final shape.

Considering springback is crucial during the design and manufacturing processes to ensure the produced parts meet the desired specifications. One of the most effective methods for reducing springback is "die compensation." [4] This method refers to the process of adjusting the design of a die to compensate for the natural tendency of the material to spring back after bending. By intentionally over-bending the material in the design of the die, the springback effect can be minimized, resulting in a finished part that meets the desired specifications. Many researchers and manufacturers have used this method to eliminate this problem. For example, Yang et al. [5] proposed a "comprehensive compensation method" (CC method) and compared it to existing compensation approaches. They evaluated the performance of the CC method on two types of sheet metal forming processes V-bending and U-bending. Their findings suggest that the CC method effectively reduces springback after a single iteration of die compensation. Similarly, Anggono et al. [6] developed a hybrid die compensation method by combining two existing algorithms displacement adjustment (DA) and spring forward (SF). A finite element analysis was conducted to simulate a U-bending forming process. This analysis investigated the springback values resulting from each compensation method across multiple computation cycles. The researchers found that the hybrid method reduced springback more effectively and required fewer compensation cycles compared to the original methods. However, while effective, die compensation can significantly increase computational time in finite element analysis. This is due to the iterative process of modifying the die surface throughout the simulation until the desired workpiece shape is achieved. Therefore, the process parameters might be optimized to minimize springback during forming before resorting to die compensation to ensure accurate workpiece geometry [7].

One of the most popular methods to optimize and analyze the optimal values are Design of Experiment (DOE) and statistical analysis methods. Researchers have used various techniques to understand and minimize springback. For instance, Thipprakmas and Phanitwong [8] investigated the influence of process parameters on springback and spring-go in V-bending using the Taguchi technique and finite element analysis. Bending angle, material thickness, and punch radius were the parameters investigated. Results indicated that bending angle had the most significant effect on both springback and spring-go, followed by material thickness and punch radius. Additionally, the Taguchi method was employed to optimize the process parameters for minimizing spring-back and spring-go. Özdemir [9] also investigated the springback behavior of DP600 steel sheets during air V bending. He analyzed the impact of four different punch tip radii and sheet thicknesses on the springback using a combined approach Taguchi's L16 orthogonal array and Response Surface Methodology (RSM). The Taguchi method identified sheet thickness as the most significant parameter affecting springback. RSM, on the other hand, allowed for visualization of the interaction between parameters and prediction of optimal settings. By employing both methods, Özdemir achieved a reduction in springback values of approximately 97.12% with the identified optimal bending parameters. Springback in U-bent metal sheets was investigated by Saravanan et al. [10] using RSM and Analysis of Variance (ANOVA). The authors analyzed the influence of punch nose radius, sheet thickness, and blank holder force on both mild steel and SS316 stainless steel. They found that all three factors significantly impact the springback angle. Additionally, significant interactions were observed between punch radius and thickness for mild steel and between blank force and thickness for stainless steel. The developed mathematical quadratic models accurately predicted the springback angle compared to the experimental results. The error between the predicted values and the experimental results was reported to be only 4.76%. Ingarao et al. [11] proposed a multi-objective approach that uses numerical simulations and RSM. They investigated the impact of friction conditions and blank holder force on both springback and thinning in DP 1000 and DP 600 steels. To identify optimal process parameters that minimize both issues, they employed Pareto optimal solution search techniques. This approach revealed that optimizing friction and strategically adjusting the blank holder force are key to reducing springback and thinning failures. However, the optimal parameters vary depending on the specific DP steel grade. This research offers valuable insights for improving the quality and consistency of stamped DP steel parts by effectively controlling springback and thinning during the forming process. Panda and Pawar [12] investigated springback in V-bending HSLA-420 steel using finite element analysis

(FEA) and Taguchi methods. Their results showed that punch angle and die opening were significant factors influencing springback, while grain direction and pre-bending had a lesser impact. By employing ANOVA analysis through Taguchi design, they were able to quantify the contribution of each parameter to springback. This approach demonstrates the effectiveness of FEA and Taguchi methods for optimizing V-bending processes and achieving better dimensional accuracy and quality in HSLA-420 components.

Recognizing the benefit of finite element (FE) simulation in predicting and addressing springback, especially offering significant time and cost savings compared to traditional trial-and-error methods [13]. Recent research has focused on utilizing FE simulations to study and overcome springback defects in AHSS forming processes. For example, Julsri et al. [14] investigated the use of the Finite Element Method (FEM) with different material models to simulate the forming process of an automotive DP780 steel part in two stages. Their results showed that the YLD89 coupled with Yoshida-Uemori hardening models were the most accurate results when compared to the experimental data. Lawanwong et al. [15] explored double action bending (DAB) as a strategy to minimize springback during DP980 steel bending. Their results showed that DAB can produce perfect hat-shaped DP980 parts without springback and the Yoshida-Uemori Model can accurately predict springback. Konzack et al. [16] used PAM-STAMP software to evaluate different material models for an S-rail part formed from AHSS DP980 steel. Their investigation revealed that a variable blank holder force, increasing from 300 kN to 4000 kN, was the most effective condition for reducing springback in the part. Chen et al. [17] investigated springback in U-channel AHSS DP600 part using ABAQUS software. They compared the accuracy of isotropic and nonlinear isotropic/kinetic hardening models. Their results showed that the nonlinear isotropic/kinesthetic hardening model produced more accurate results. This study suggests that the Bauschinger effect has a significant influence on springback simulations. In a similar, Tong and Van Canh [18] investigated the accuracy of a proposed combined hardening model for predicting springback in U-draw bending of DP350 steel sheets. They compared this model to traditional isotropic and kinematic hardening models. Their results demonstrated that the combined approach offered better prediction accuracy. Further analysis of process parameters revealed that the sidewall radius was the most sensitive factor influencing springback. Increasing the punch and die radius tended to increase springback, while a higher blank holder force resulted in a decrease. The clearance between the die and punch had a negligible influence on springback. Moreover, Chongthairungruang et al. [19] compared the springback prediction of three material models with experimental results from a U-shaped forming process. They investigated two dual-phase steels, JSC590R and JSC780Y, and one mild steel, JSC270C. Their results showed that the Yoshida-Uemori model provided the most accurate predictions, especially for the higher-strength DP steels. This is because the Yoshida-Uemori model accounts for the kinematic hardening behavior of the material, which is more significant for high strength steels compared to mild steels. Finally, Hassan et al. [20] investigated springback prediction in deep drawing simulations of DP600 steel. They proposed a method to generate multiple cyclic stress-strain curves with varying pre-strain levels from a single experiment. They developed an enhanced finite element model that incorporates these curves. The model assigns the relevant stress-strain curve to each element based on its pre-strain level after each calculation step. This approach was then compared to conventional methods that utilize a single stress-strain curve and more complex hardening models. The results demonstrated that the new method achieves significantly better accuracy in predicting springback for both hat and tunnel geometries.

Building upon this extensive body of research, this study aims to identify the most suitable material model for accurately predicting the forming behavior of a 1 mm-thick AHSS grade JSC980Y automotive panel by investigating the accuracy of four material models, each combining a yield criterion (Hill 1948 or Barlat 1989) with a hardening rule (Swift or Yoshida-Uemori). These specific models were chosen based on their common use in sheet metal forming simulations and their potential to accurately capture the anisotropic behavior and Bauschinger effect observed in AHSS materials during a stamping process using advanced finite element simulation techniques. The "Best Fit" method will be employed to locate and compare the simulation results with the 3D mesh obtained by scanning the physical part. The analysis will focus on summarizing the percentage of area in the displacement range. The selected material model will be used to simulate an experiment to collect all combination parameters within a Taguchi L_{27} (3^3) orthogonal array for best reliability results. The chosen process parameters for this experiment are blank holder force, die gap, and blank width. An analysis of variance (ANOVA) will be used to analyze the effect of each process parameter and to differentiate their significance. A multiple regression analysis was used to develop a mathematical equation for predicting optimal process parameters. While existing research [21-23] has investigated the application and comparative performance of various regression models for springback prediction across different cases, but regression model is dependent upon the relationships between the data variables. A quadratic model may offer a better fit compared to a simple linear model. However, overfitting must be considered if the model complexity exceeds that of the data [24-25]. The chosen model was selected for its ability to accurately predict the optimal combination of the three identified process parameters and subsequently validated through simulation.

DOI:10.4186/ej.2024.28.10.25

2. Experiment Setup

2.1. Workpiece

This paper selects the automotive body part 'Bow-RF Panel' as a case study. This workpiece is produced from advanced high strength steel grade JSC980Y with a thickness of 1 mm. The panel part is produced using five processes: drawing, trimming, CAM-trimming, restriking, and separating. This work focuses only on the drawing process which experiences a strong springback after forming. The machine used to form this workpiece is a Simpac Hydraulic press 800T with the following specifications: press capacity 800 tons, stroke and daylight length 1500mm, Bolster & Slide Dimensions 3000x2000 mm, Die Cushion Capacity 250 tons, Die Cushion Stroke 350 mm. Fig. 1 shows the Bow-RF Panel part.

Fig. 1. Automotive body part Bow-RF Panel.

2.2. Material Properties & Testing

In this study, the material's properties are characterized using uniaxial tensile testing and tension-compression cyclic testing. Material parameters are determined using these techniques for a difference of material models such as the Hill 1948 yield criterion, the Barlat 1989 yield criterion, the Swift hardening model, and the Yoshida-Uemori hardening model.

2.2.1. Uniaxial tensile testing

Uniaxial tensile testing is a fundamental material testing method that applies a tensile load in a single direction until the material failure. This test is performed to obtain key mechanical properties of a material and determine parameters used in simulation models such as the Hill 1948 yield criterion, the Barlat 1989 yield criterion, the Swift hardening model, and the Yoshida-Uemori hardening model. The tensile testing was conducted using a universal testing machine with a constant crosshead velocity of 0.05 mm/s. A Digital Image Correlation (DIC) optical camera was employed to collect data during the testing process. The DIC system essentially tracks tiny speckles or patterns painted on the specimen to calculate the precise deformation. Specimens for the experiment were prepared using Computer Numerical Control (CNC) wire cutting. This ensures precise dimensions and a smooth surface. Three different directions were chosen for specimen preparation: 0°, 45°, and 90° angles relative to the rolling direction to investigate how the material's properties vary depending on the orientation. The true stress-strain curve obtained from the test is shown in Fig. 2. Key mechanical properties, including Young's modulus (E), yield strength (YS), ultimate tensile strength (UTS), and uniform elongation (ε_u), were extracted from the tensile test results for each testing direction and are presented in Table 1.

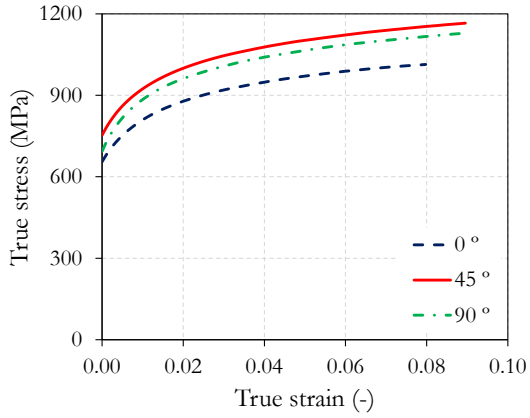

Fig. 2. True stress-strain curves of JSC980Y steel for each direction.

Table 1. Mechanical properties of the JSC980Y under uniaxial tensile testing.

Directions	E (GPa)	YS (MPa)	UTS (MPa)	ε_u (%)
0 °	189	656	936	9.04
45 °	188	759	1066	10.1
90 °	190	710	1032	10.04

2.2.2. Tension-compression testing

Tension-compression testing is the material properties method that applies a tensile load and applies the opposite compression load to the specimen in a cycle loop. This testing is crucial for material characterization, specifically in determining the Yoshida-Uemori mixed kinematic hardening rule. The established model accurately predicts springback by capturing the Bauschinger effect [26] during the drawing process, which involves loading a material in opposite directions. The experiment used a fixture to hold the specimen to prevent buckling from occurring while testing. Apply dry film lubricant to the contact surface between the specimen and the fixture to prevent contact friction related errors in the results. The fixture was attached to the specimen with coil spring force [27]. A DIC camera is used for collecting the local displacement value of the specimen while testing. The resulting cyclic true stress-strain curve obtained from the testing is presented in Fig. 3.

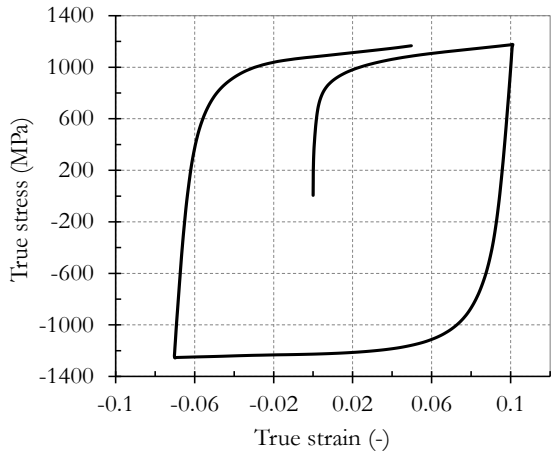

Fig. 3. True stress-strain cyclic curve of JSC980Y steel from tension-compression testing.

2.3. Material Models

To Accurately capture the mechanical behavior of sheet metals, particularly AHSS grades for predicting and minimizing springback in forming simulations. The choice of yield criterion and hardening rule significantly influences the accuracy of these simulations. This study investigates four material models, each model combining a yield criterion with a hardening rule to identify the most suitable model for predicting the behavior of JSC980Y AHSS during stamping.

2.3.1. Yield Criterion

2.3.1.1 Hill 1948 Yield Criterion

The Hill 1948 yield criterion [28], developed by Rodney Hill, is a widely used and convenient model for simulating plastic deformation in anisotropic sheet metals. Building upon the Huber-Mises-Hencky criterion [29], it employs a quadratic equation to account for the material's directional properties. This approach considers the tensile and shear yield stresses in different directions, assuming the material exhibits anisotropy with three orthogonal planes of symmetry. The Hill 1948 criterion offers valuable insights into material behavior under stresses exceeding the elastic limit. By incorporating the material's directional preferences for deformation, it offers a deeper understanding of plastic behavior in sheet metal forming simulations. The specific mathematical form of the Hill 1948 yield criterion can be represented by the following equation:

$$\begin{aligned} 2f(\sigma_{ij}) \equiv\ & F(\sigma_{yy}-\sigma_{zz})^2 + G(\sigma_{zz}-\sigma_{xx})^2 \\ & + H(\sigma_{xx}-\sigma_{yy})^2 + 2L\sigma^2{}_{yz} \\ & + 2M\sigma^2{}_{zx} + 2N\sigma^2{}_{xy} = 1 \end{aligned} \quad (1)$$

The yield function is denoted by f, where parameters $F, G, H, L, M,$ and N are material constants representing the state of anisotropy. $x, y,$ and z correspond to the principal anisotropic axes. In the case of sheet metal forming, the x - axis typically aligns with the rolling direction, the y - axis aligns with the transverse direction and the z - axis aligns with the thickness of the material. Under plane stress conditions$(\sigma_{zz} = \sigma_{zx} = \sigma_{yz} = 0)$ the equation can be expressed as

$$\begin{aligned} 2f(\sigma_{ij}) \equiv\ & (G+H)\sigma^2{}_{xx} - 2H\sigma_{xx}\sigma_{yy} \\ & + (H+F)\sigma^2{}_{yy} + N\sigma^2{}_{xy} \\ & = 1 \end{aligned} \quad (2)$$

When using the Hill 1948 yield criterion in sheet forming simulation, R-value based method serves as the chosen approach for identifying the material parameters associated with the yield criterion. Lankford coefficients $(r_0, r_{45}$ and $r_{90})$ are utilized based on the established relationship between the constants $F, G, H,$ and N. This relationship aligns with that obtained from the flow rule, as presented in the following equations:

$$F = \frac{r_0}{r_{90}(1+r_{90})} \quad (3)$$

$$G = \frac{1}{(1+r_0)} \quad (4)$$

$$H = \frac{r_0}{(1+r_0)} \quad (5)$$

$$N = \frac{(r_0+r_{90})(1+2r_{45})}{2r_{90}(1+r_0)} \quad (6)$$

In this work, r-values were obtained from uniaxial tensile test conducted in three directions. These values are subsequently incorporated as input parameters for the yield criterion within the material model used for the simulation. The specific r-values are tabulated in Table 2.

Table 2. Lankford coefficients (r-values) in three directions.

Directions	r-values
0°	0.82
45°	0.83
90°	0.92

2.3.1.2 Barlat 1989 Yield Criterion

The Barlat-Lian yield criterion [30], proposed in 1989, is a non-quadratic model that extends Hosford's criterion [31]. It is formulated in a non-orthogonal $x, y,$ and z coordinate system, allowing for a more general description of material behavior. In normal anisotropy form, the yield function is defined by specific coefficients within the equation.

$$f = a|k_1 + k_2|^M + a|k_1 - k_2|^M + c|2k_2|^M = 2{\sigma_e}^M \quad (7)$$

where k_1 and k_2 were given by

$$k_1 = \frac{\sigma_{11} + h\sigma_{22}}{2} \quad (8)$$

$$k_2 = \sqrt{\left(\frac{\sigma_{11} - h\sigma_{22}}{2}\right)^2 + p^2{\sigma_{12}}^2} \quad (9)$$

Material parameters a, c, h, and p were identified by

$$a = 2 - c = \frac{2\left(\frac{\sigma_e}{\tau_{s2}}\right)^M - 2\left(1 + \frac{\sigma_e}{\sigma_{90}}\right)^M}{1 + \left(\frac{\sigma_e}{\sigma_{90}}\right)^M - \left(1 + \frac{\sigma_e}{\sigma_{90}}\right)^M} \quad (10)$$

$$h = \frac{\sigma_e}{\sigma_{90}} \quad (11)$$

$$p = \frac{\sigma_e}{\tau_{s1}}\left(\frac{2}{2a + 2^M c}\right)^{\frac{1}{M}} \quad (12)$$

With τ_{s1} and τ_{s2} are yield stress in two difference shear tests. While M = 6 for Body-Centered Cubic (BCC) materials and M = 8 for Face-Centered Cubic (FCC) materials. An alternative, simpler procedure relies on r-values obtained through:

$$a = 2 - c = 2 - 2\sqrt{\frac{r_0}{1 + r_0}.\frac{r_{90}}{1 + r_{90}}} \quad (13)$$

$$h = \sqrt{\frac{r_0}{1 + r_0}.\frac{1 + r_{90}}{r_{90}}} \quad (14)$$

The material parameters employed within the Barlat 1989 yield criterion for this study are presented in Table 3. These parameters were derived from the corresponding material testing results.

Table 3. Material parameters for Barlat 1989 model.

a	c	h	p	M
1.06	0.94	0.95	0.96	6

In this study, the Hill 1948 and Barlat 1989 yield criteria were selected due to their widespread use in sheet metal forming simulations and proven ability to represent anisotropic material behavior. This selection is supported by numerous studies that have demonstrated the effectiveness of these models for predicting formability and springback in various sheet metal forming processes [32-35]. The Hill 1948 model offers a relatively simple and computationally efficient approach for capturing anisotropy, while the Barlat 1989 model provides a more sophisticated representation, particularly for materials exhibiting complex yielding behavior.

2.3.2. Hardening Model

2.3.1.3 Swift model

Swift hardening law or Krupkowski hardening law is a hardening equation that is widely used to describe plastic behavior in sheet metal simulation. It is easy to use and can accurately describe the behavior of materials. The hardening curve can be described by the equation [36]:

$$\sigma = K\left(\varepsilon_p + \varepsilon_0\right)^n \quad (15)$$

where K is the material constant, ε_p is the plastic strain, ε_0 is the offset true strain, and n is the strain hardening exponent.

2.3.3. Yoshida-Uemori hardening model

The Yoshida-Uemori (Y-U) hardening model [26], proposed by Yoshida and Uemori, builds upon the Chaboche model [37] to describe the cyclic deformation behavior of materials undergoing large-strain cyclic plasticity. This constitutive model employs a two-surface framework, where both the yield surface and the bounding surface can evolve in size and position. However, the bounding surface always encompasses the yield surface. The Y-U model utilizes kinematic hardening for the yield surface within a mixed isotropic-kinematic hardening framework for the bounding surface. This approach enables the model to accurately capture the transient Bauschinger effect and various cyclic hardening characteristics, including strain-range dependence and work hardening stagnation. The specific formulation of the yield surface function f is given by:

$$f = \sqrt{\frac{3}{2}}\|s - \alpha\| - Y = 0 \quad (16)$$

where s is the Cauchy stress tensor of yield surface, α is the backstress tensor of yield surface, and Y is initial yield stress which represents the radius of yield surface. Mathematically, the bounding surface function F is formulated as:

$$F = \sqrt{\frac{3}{2}}\|s - \beta\| - R - B = 0 \quad (17)$$

where β represents the backstress, which defines the center of the bounding surface. B denotes the initial size of the bounding surface. R is the amount of isotropic hardening of the bounding surface. In the context of kinematic hardening, the relative motion of the yield surface with respect to the bounding surface is described by:

$$\alpha_* = \alpha - \beta. \tag{18}$$

The Y-U model describes the hardening behavior during plastic deformation through the evolution of the yield surface. This evolution is mathematically expressed by:

$$\dot{\alpha_*} = C\left[\left(\frac{a}{Y}\right)(\sigma - \alpha) - \sqrt{\frac{a}{\alpha_*}}\alpha_*\right]\dot{p} \tag{19}$$

The equation also includes with a material parameter that controls the rate of kinematic hardening (C), the Cauchy stress of yield surface (σ), the effective plastic strain rate $(\dot{p})$, and the difference size between the yield surface and bounding surface (α) that is governed by the following equation:

$$a = B + R - Y \tag{20}$$

For mixed isotropic-kinematic hardening of the bounding surface section, the isotropic hardening evolution of the bounding surface equation is described by the equation:

$$\dot{R} = m(R_{sat} - R)\dot{p} \tag{21}$$

where m is material parameter that control isotropic hardening rate and R_{sat} is the saturated parameter of R value. The evolution of the bounding surface during kinematic hardening is described by the following equation:

$$\dot{\beta} = m\left[\left(\frac{b}{Y}\right)(\sigma - \alpha) - \beta\right]\dot{p} \tag{22}$$

where b is a saturated parameter of β. However, limitations arise when applied to very large plastic strain ranges. To address this, modifications were made to the original model to capture work hardening behavior in these high strain regions and prevent premature saturation. The revised equation takes the following form:

$$\mathrm{R} = R_{\mathrm{sat}}\left[(C_1 + p)^{C_2} - C_1^{C_2}\right] \tag{22}$$

Material parameters C_1 and C_2 are material parameters that controls the rate of the kinematic hardening. The parameter h captures the work hardening stagnation observed during reverse loading. This parameter is calibrated through numerical simulations of cyclic stress-strain behavior to ensure consistency with the experimental data. In this work. The Y-U parameter $(Y, B, m, b, R_{sat}, C_1, C_2, h)$ that used for predicting drawing part from JSC980Y was identified and shown in Table 4.

Table 4. Material parameters for the Y-U model.

***Y* (MPa)**	***B* (MPa)**	***m***	***b* (MPa)**
708.44	962.27	7.58	193.37
R_{sat} (MPa)	**C_1**	**C_2**	**h**
203.27	225	141	0.5

After obtaining the Y-U parameters from the above methods, the results found that all of the early re-plastination was not covered by the description. The degradation of the elastic modulus was identified, and the additional elastic modulus parameters were incorporated with a mathematical model [38]:

$$E = E_0 - (E_0 - E_a)[1 - exp(-\xi p)] \tag{23}$$

where E_0 and E_a are Young's modulus at the initial stage and infinitely large pre-strained materials, subsequently. ξ is material constant. In this work, elastic modulus degradation parameters were listed in Table 5.

Table 5. Elastic modulus parameters for the Y-U model. [27]

E_0 (GPa)	**E_{sat} (GPa)**	**ξ**
189	128.40	14.19

In this work, the Swift and Yoshida-Uemori hardening rules were selected to represent the isotropic and combined isotropic-kinematic hardening behavior of the JSC980Y AHSS, respectively. This selection is based on previous studies that have highlighted the importance of incorporating the Bauschinger effect for accurate springback prediction in AHSS and have compared the results obtained with the Yoshida-Uemori model to those obtained with the Swift model [39-42]. The Swift model provides a straightforward approach to describe strain hardening, while the Yoshida-Uemori model accounts for the Bauschinger effect, a phenomenon often observed in AHSS materials that significantly influences springback prediction.

2.4. Finite Element Simulation

The finite element (FE) simulation stage employed commercial software, PAM-STAMP 2022, to predict the drawing process of the automotive Bow-RF panel. The standard stamping module with the PAM-Autostamp solver was used for this analysis. Tooling components, including the die, blank holder, and punch were set up as rigid bodies to reflect their structural stiffness during forming. The simulation was divided into four distinct stages: gravity, closing, forming, and springback, respectively. To ensure prediction accuracy, the blank mesh was initially set to a size of 12 mm and then refined to a final size of 0.8 mm with a maximum of five refinement levels. Additionally, a dedicated refinement level of four was applied along the blank's outline for enhanced detail capture. The calculation type for the gravity and springback stages was set to "advanced implicit" due to their emphasis on static behavior. Conversely, the closing and forming stages, involving dynamic interactions, utilized an "explicit" solver setting [43]. Table 6 presents the established consistent process parameters. Figure 4 illustrates the 3D finite element models of the die, punch, and blank holder.

Table 6. Basic process parameters used for simulation.

Stamping velocity (mm/ms)	Stroke (mm)	Coefficient of friction	Blank Holder Force (tons)
5	50	0.125	35

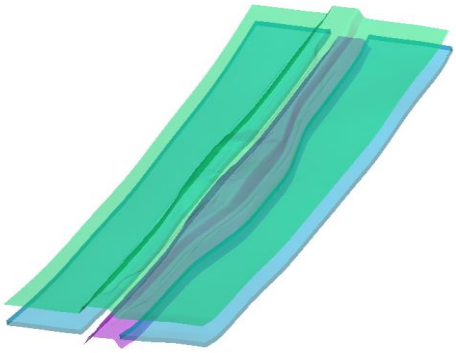

Fig. 4. FE tool and blank models using the PAM-STAMP software.

To identify the model that gives the most accurate results, a comparative evaluation of four material models that integrate yield criteria and hardening laws was conducted. These models are detailed in Table 7.

Table 7. Combination of yield criterion and hardening law used in the study.

Yield criterion	Hardening law
Hill 1948	Swift
Barlat 1989	Swift
Hill 1948	Yoshida - Uemori
Barlat 1989	Yoshida - Uemori

2.5. Measurement Method

This work achieved two key goals: selecting the most accurate material models for the experiment and determining the optimal process parameters that minimize springback on the workpiece. This minimization was measured by the percentage of the area of displacement deviation between the simulated and reference parts. To compare the ability of each material model, an actual workpiece was formed and scanned using a portable 3D scanner, the Go! Scan 3D. The scanned data was then generated by the CREAFORM software. After receiving the scanned CAD file data, the scanned model was imported into PAM-STAMP software and positioned identically to the simulation result using the "Bestfit" [43] feature. Figure 5 presents both 3D models. The displacement between the scanned part and the simulation result was analyzed and presented as a percentage of the area in each displacement range. The 3D model contour also shows the difference in color within each range. Following the material model comparison, finding the optimal parameter using statistical methods involved measuring the same quantities mentioned above. In this case, the authors compared the simulated shape with the target shape to assess the degree of shape distortion. This analysis was then used to find the set of parameters that minimized the distortion of the workpiece.

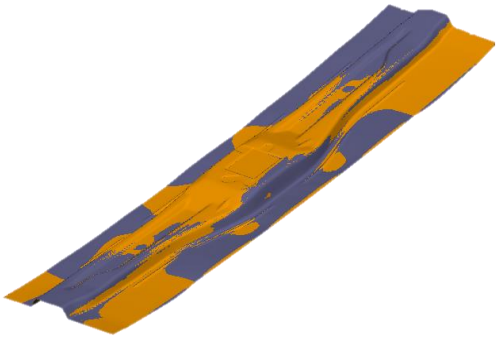

Fig. 5. Scanned model and simulation result at same position with Bestfit.

2.6. Taguchi Method & Experiment Design

After determining the suitable material model that yielded the most accurate results for the current work, the second objective was to optimize process parameters to

minimize shape distortion from the springback effect or improve dimensional accuracy before compensation in the design phase. The Taguchi robust design method was employed. This methodology is a powerful approach to the robust design of experiments used to optimize products and processes. It offers several benefits, such as improved product quality, reduced process cost, and a minimized number of experiments [44-45], through the use of orthogonal arrays (OA) [46]. In Taguchi design, control factors are manipulated, and noise factors (uncontrollable factors) are varied. The goal is to find control factor settings that make a product or process robust to noise. A signal-to-noise ratio (S/N) [47] is a key metric used to identify the optimal settings. Higher S/N values indicate less impact from noise. A two-step optimization process refines these settings: first minimizing variability, then adjusting the mean to the target value while maintaining low noise impact. Different S/N ratios are used depending on the experiment's goals. The S/N ratio can be categorized into three main types [46, 48], as shown in the following equations:

Nominal the best

$$S/N = 10\,log\frac{\bar{y}^2}{s^2} \tag{24}$$

Larger is better

$$S/N = -10\,log\left(\frac{1}{n}\sum_{i=1}^{n}\frac{1}{y_i^2}\right) \tag{25}$$

Smaller is better

$$S/N = -10\,log\left(\frac{1}{n}\sum_{i=1}^{n}y_i^2\right) \tag{26}$$

where y is responses, $\bar{y}$ is mean of responses, S is standard deviation of the responses, and n is number of responses. In this research, MiniTab 21 software was used for data analysis. Three process parameters were chosen as the control factors: blank holder force (A), die gap (B), and blank width (C). Each factor included three distinct levels: low, medium, and high, as detailed in Table 8. The medium level corresponds to the original process parameter that was used in production.

These factors were optimized by using Taguchi's OA L_{27} (3^3) [49] that is presented in Table 9. The total number of runs for this analysis is 27. For the experimental design, the influence of the interaction and second-order terms between each factor will also be analyzed in this experiment. The objective of the analysis is to find the optimal values of the variables that minimize the distortion of the workpiece. In this case, the percentage of area of displacement in the range of -1 to 1 mm between the desired workpiece shape and the simulated workpiece shape is maximized. Therefore, this experiment employs the Taguchi S/N ratio analysis, which emphasizes the importance of larger dimensions.

Table 8. Selected factors and values at each level.

Process parameter	Units	Levels		
		1	2	3
Blank holder force	Tons	20	35	50
Die gap	mm	0.9	1	1.1
Blank width	mm	290	300	310

Table 9. Taguchi L_{27} (3^3) orthogonal array.

Experiment No.	Factor's levels		
	A	*B*	*C*
1	1	1	1
2	1	1	2
3	1	1	3
4	1	2	1
5	1	2	2
6	1	2	3
7	1	3	1
8	1	3	2
9	1	3	3
10	2	1	1
11	2	1	2
12	2	1	3
13	2	2	1
14	2	2	2
15	2	2	3
16	2	3	1
17	2	3	2
18	2	3	3
19	3	1	1
20	3	1	2
21	3	1	3
22	3	2	1
23	3	2	2
24	3	2	3
25	3	3	1
26	3	3	2
27	3	3	3

DOI:10.4186/ej.2024.28.10.25

3. Experimental Results and Analysis

3.1. Comparison of Material Models for Springback Simulation Accuracy

In this study, the accuracy of different material models is compared and listed in Table 7. The comparison results were evaluated to determine the most suitable model for optimizing process parameter. The simulation results, obtained using the same process parameters as the actual process (as shown in Table 6) after the springback stage, were compared with a 3D model of the actual formed part that was scanned. The contour used to evaluate the accuracy of the simulation results was the displacement between the two parts. The percentage of area in each displacement range was analyzed, including ranges of more than -5 mm, -5 to -3 mm, -3 to -1 mm, -1 to 1 mm, 1 to 3 mm, 3 to 5 mm, and more than 5 mm, compared to the total area of the workpiece. Figure 6 presents a color-coded displacement map comparing the simulation results with the actual formed part. The displacement ranges are represented by different colors: dark blue for areas with displacement greater than -5 mm, blue for areas between -5 mm and -3 mm, light blue for areas between -3 mm and -1 mm, green for areas between -1 mm and 1mm, yellow for areas between 1mm and 3 mm, red for areas between 3 mm and 5 mm, and dark red for areas with displacement greater than 5 mm.

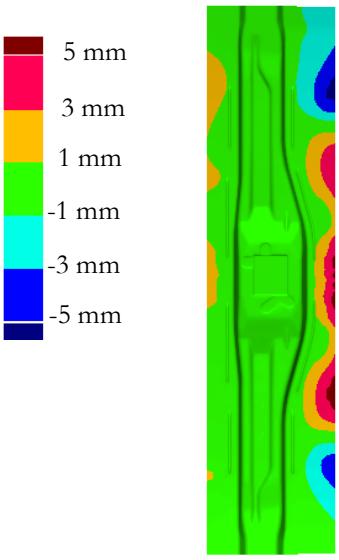

Fig. 6. Color map model of displacement between actual and simulated part result.

Figure 7 shows the area percentage of displacement between the simulation results and the actual workpiece in each range, divided into ranges and displayed as a histogram. From the experimental results in Fig. 7(a), it was found that in the range of -1 to 1 mm, which is the range with the least error, the use of Barlat 1989 and Y-U together had the highest value of 83.17%, followed by the Hill 1948 model together with Y-U at 81.64%. In the displacement ranges of 1 to 3 mm, 3 to 5 mm, and more than 5 mm, as shown in Fig. 7(b) to 7(d), it was found that in the ranges with more error in the positive value range, the models using Y-U tended to have less than other models. It was also found that Barlat 1989 together with Y-U had the least error. In the displacement range of negative values between -1 to -3 mm, -3 to -5 mm, and more than -5 mm, as shown in Fig 7(e) to 7(g), it was found that overall, the models using Swift could predict with slightly less error than the models using Y-U.

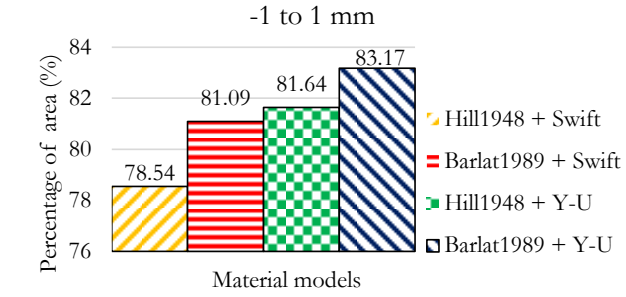

(a)

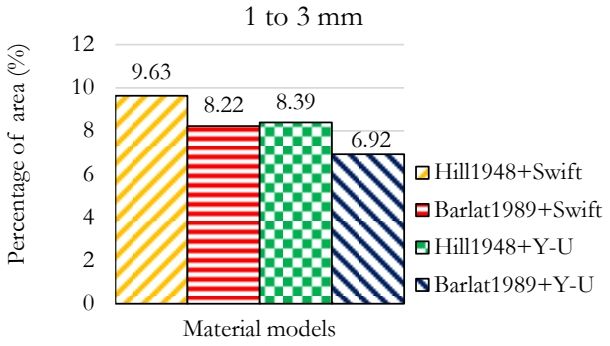

(b)

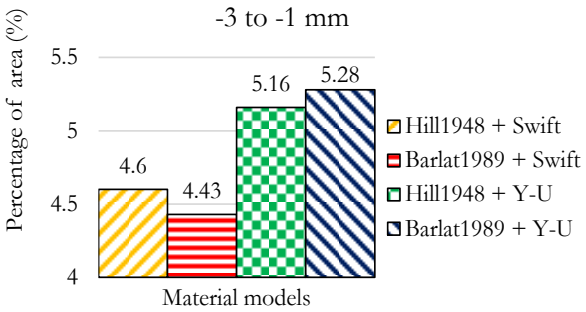

(c)

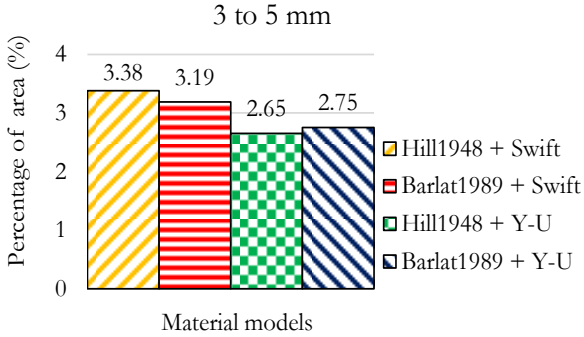

(d)

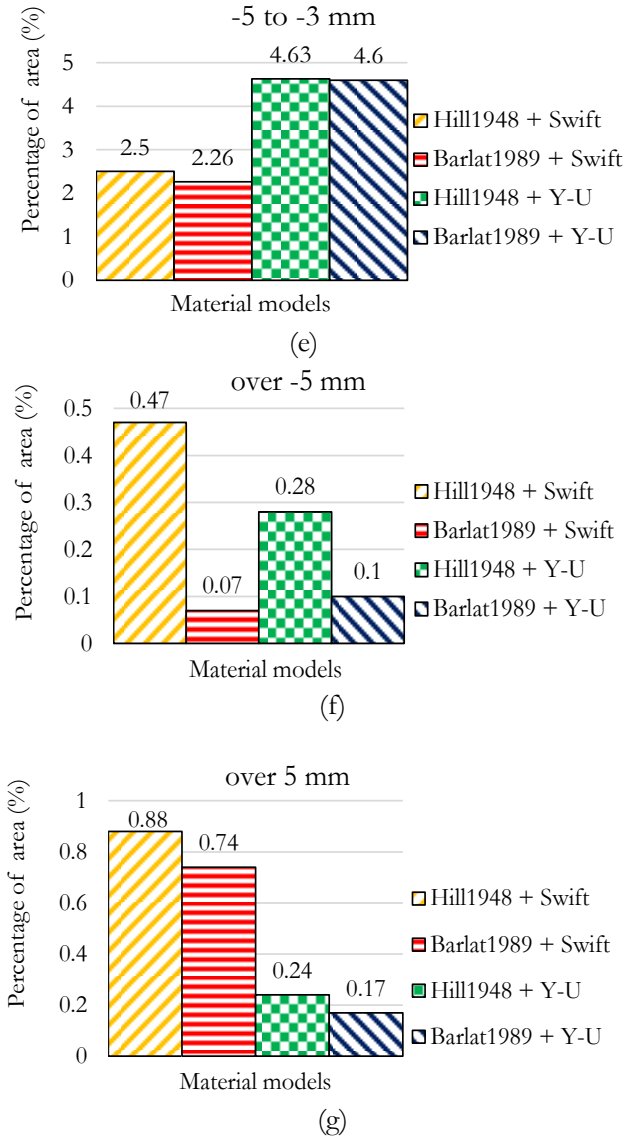

Fig. 7. Percentage of area comparison in (a) -1 to 1 mm, (b) -3 to -1 mm, (c) 1 to 3 mm, (d) -5 to -3 mm, (e) 3 to 5 mm, (f) over -5 mm, and (g) over 5 mm.

In summary, the experimental results showed that using Barlat 1989 and Y-U together had the least error in the displacement range of -1 to 1 mm. In the displacement ranges of 1 to 3 mm, 3 to 5 mm, and more than 5 mm, the models using Y-U tended to have less error than other models. In the displacement range of negative values between -1 to -3 mm, -3 to -5 mm, and more than -5 mm, the models using Swift could predict with slightly less error than the models using Y-U. In this research, the Barlat 1989 and Y-U material models were selected for the optimization experiment to find the most suitable process parameters. This is because these models provide the highest accuracy in the low-error range and, overall, can provide more accurate results than other material models.

Table 10. The total Taguchi L_{27} experiment run results with S/N ratio.

Blank Holder Force (tons)	Die Gap (mm)	Blank Width (mm)	Percentage (%)	S/N Ratio (dB)
20	0.9	290	83.54	38.44
20	0.9	300	82.93	38.37
20	0.9	310	81.69	38.24
20	1	290	83.58	38.44
20	1	300	83.76	38.46
20	1	310	81.12	38.18
20	1.1	290	79.22	37.98
20	1.1	300	79.53	38.01
20	1.1	310	79.5	38.01
35	0.9	290	86.64	38.75
35	0.9	300	86.79	38.77
35	0.9	310	84.55	38.54
35	1	290	84.01	38.49
35	1	300	85.61	38.65
35	1	310	84.11	38.50
35	1.1	290	80.74	38.14
35	1.1	300	83.48	38.43
35	1.1	310	81.25	38.20
50	0.9	290	86.05	38.70
50	0.9	300	85.76	38.67
50	0.9	310	85.54	38.64
50	1	290	83.72	38.46
50	1	300	84.72	38.56
50	1	310	84.35	38.52
50	1.1	290	78.89	37.94
50	1.1	300	80.35	38.10
50	1.1	310	81.59	38.23

3.2. Analysis of Taguchi method

An experimental study using the Taguchi method was conducted to investigate the effects of blank holder force, die gap, and blank width on the percentage of area with displacement in the range of -1 to 1 mm between the desired workpiece shape and the simulated workpiece shape at the same position, compared to the total area of the workpiece. This range was selected as the acceptable tolerance for dimensional accuracy in the formed part. The objective was to maximize the percentage of area within this range, thereby minimizing springback and

improving the overall part quality. A total of 27 individual trials were performed based on the Taguchi L_{27} orthogonal array. The results were analyzed using the Signal-to-Noise (S/N) ratio.

In this study, the "larger-the-better" S/N ratio characteristic was chosen for the analysis because the goal is to maximize the percentage of area within the desired displacement range (-1 to 1 mm). Table 10 lists all experimental of the L_{27} Taguchi table. It details the response values (percentage of area) and the corresponding calculated S/N ratios for each experiment conducted under various combinations of the three investigated parameters.

The average response at each level and the delta value in Table 11 determine the influence of each control factor. The delta value represents the difference between the highest and lowest average responses of each level for that factor. The delta value can also indicate the influence of that factor on the response. A factor with a high delta value has a high influence on the response. Therefore, Table 11 shows that the die gap has the highest influence on the response, followed by the blank holder force and blank width, respectively. Figure 8 and 9, calculated from the mean and S/N ratio, respectively. These graphs show the influence of each factor on the percentage of area.

Table 11. Average response and delta value for each control factor.

Level	Blank holder force (tons)	Die Gap (mm)	Blank Width (mm)
1	81.65	84.83	82.93
2	84.13	83.89	83.66
3	83.44	80.51	82.63
Delta	2.48	4.33	1.03
Rank	2	1	3

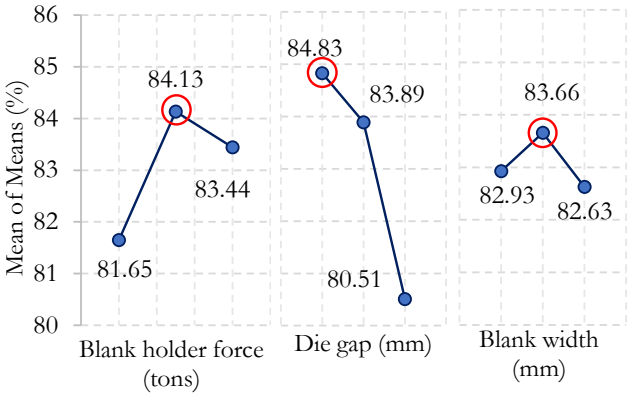

Fig. 8. Main factor effect of mean.

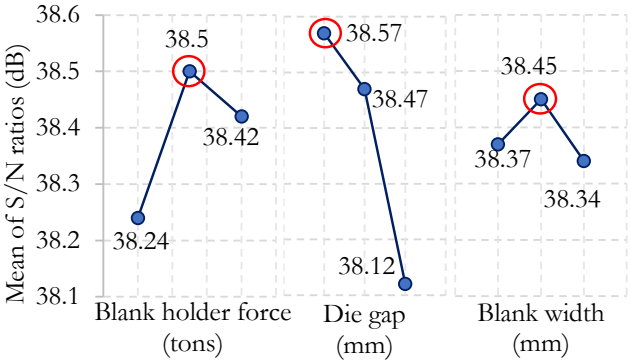

Fig. 9. Main factor effect of S/N ratio.

From these results, it was found that the levels with the highest mean and S/N ratio values (marked with circles) were blank holder force at level two, die gap at level one, and blank width at level two. Using the Taguchi method, the optimal parameters from the experiment were found to be A = 35 ton (level 2), B = 0.9 mm (level 1), and C = 300 mm (level 2). After obtaining the optimal parameters from the above analysis, the percentage of area was predicted using the Taguchi's confirmation test using equation 27. However, the effects of interaction were also considered becasuse there were interaction effects [50]. Figure 10 shows the interaction of each factor when the relationship lines of each variable are not parallel or intersect. It indicates that there is an interaction between the factors. The influence of the interaction between all factors was statistically significant at the 95% confidence level according to the ANOVA [45, 50] table in Table 13.

3.3. Analysis of Taguchi Method

To predict the response value from the optimal variables obtained from the Taguchi analysis method, where all factors are significant including the interaction effect, the average response value of all factors will be calculated using the following equation [44]:

$$\begin{aligned} \%Area = \bar{T} &+ (\overline{A_2B_1} - \bar{T}) + (\overline{B_1C_2} - \bar{T}) \\ &+ (\overline{A_2C_2} - \bar{T}) - (\overline{A_2} - \bar{T}) \\ &- (\overline{B_1} - \bar{T}) - (\overline{C_2} - \bar{T}) \end{aligned} \quad (27)$$

where $\bar{T}$ is total average result, $\overline{A_2}$ is average effect of factor A at level 2, $\overline{B_1}$ is average effect of factor B at level 1, $\overline{C_2}$ is average effect of factor C at level 2, $\overline{A_2B_1}$ was average combination effect of factor A at level 2 and factor B at level 1, $\overline{B_1C_2}$ is average combination effect of factor B at level 1 and factor C at level 2, and $\overline{A_2C_2}$ is average combination effect of factor A at level 2 and factor C at level 2. From Taguchi L_{27} Table 10 Thus,

$\bar{T} = 83.07$, $\overline{A_2} = 84.13$, $\overline{B_1} = 84.83$, $\overline{C_2} = 83.66$, $\overline{A_2B_1} = 86$, $\overline{B_1C_2} = 85.16$, and $\overline{A_2C_2} = 85.3$

Substituting all term to Eq. (27),

$$\%Area = 86.9\%$$

From the predicted values of the above equation, the accuracy of the prediction results was confirmed by comparing the obtained values with those obtained from the experiment in Table 12. The analysis showed a 0.13% error between the prediction results and the experiment values. When compared with the results of using the original process parameters, the parameters obtained from the analysis gave a percentage of area that was 1.38% higher.

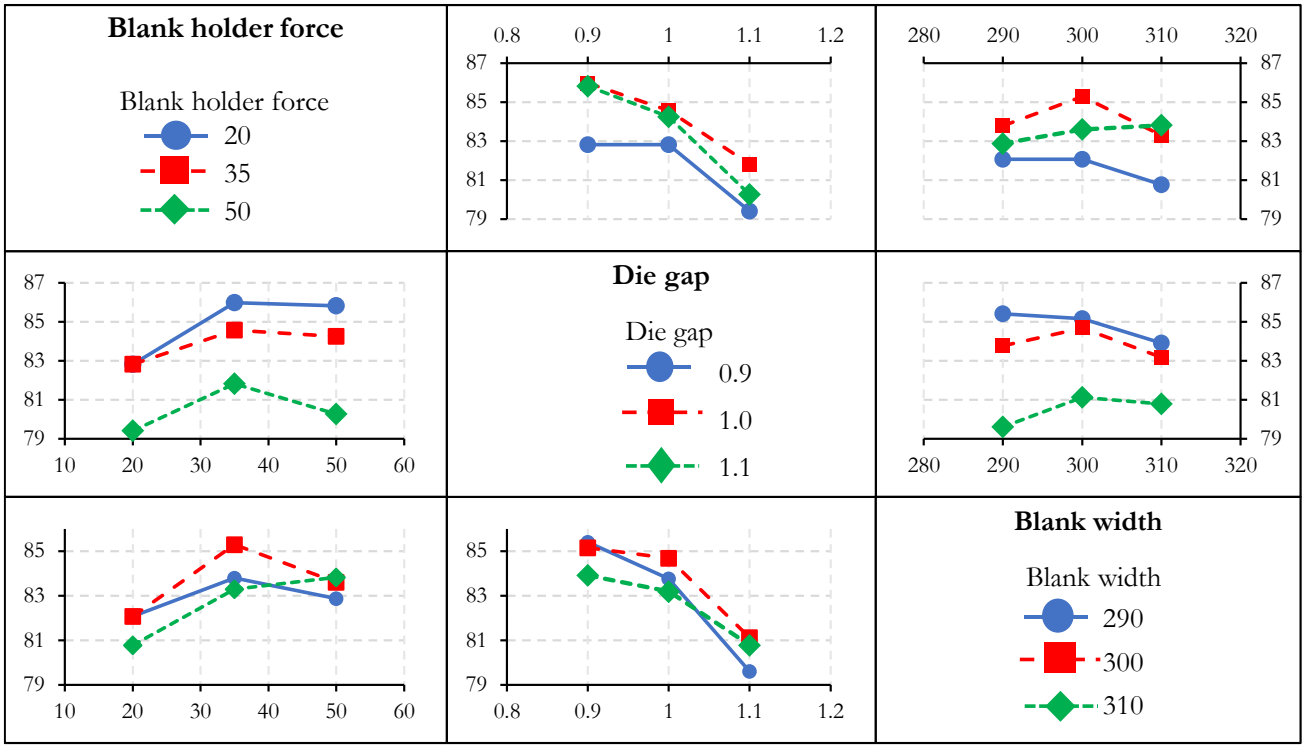

Fig. 10. The influence of each factor's interaction on the average percentage of area.

Table 12. Taguchi optimal parameter confirmation test.

	Initial parameter	Optimized parameter	
		Predicted parameter	Experiment parameter
level	$A_2B_2C_2$	$A_2B_1C_2$	$A_2B_1C_2$
% area	85.61	86.90	86.79
% difference	-	0.13	-
improvement	1.18	-	-
% improvement	1.38	-	-

3.4. ANOVA Method

After analyzing the optimal variables from the experimental and studying the influence of the experimental variables using Taguchi, ANOVA [51] was used as a statistical analysis tool to investigate the influence of various variables by analyzing the process robustness to noise factors (S/N ratio) [45, 50]. The main factors, including blank holder force, die gap, and blank width, as well as the interactions between each factor, were analyzed and conducted at a 95% confidence level. P-values were used to determine the statistical significance of each variable's effect on the S/N ratio. Additionally, the percentage contribution of each variable was calculated to quantify its relative impact. Table 13 displays the ANOVA results.

Where DF represents degrees of freedom, seq SS represents sequential sums of squares, and adj SS represents adjusted sums of squares. The F-value is a statistical test tool to determine the term associated with the response. The P-value is a probability that is calculated from the F-value and used to evaluate the evidence against the null hypothesis. In this case, a significance level of 0.05 was used. The S/N ratios, influenced by blank holder

force, die gap, and blank width, the interaction between blank holder force and die gap, the interaction between blank holder force and blank width, and the interaction between die gap and blank width, are represented with the percentage of contribution consisting of 19.89%, 63.65%, 3.34%, 3.19%, 4.37%, 4.1%, and 1.47%, respectively. The results showed that the die gap was the most influential factor, followed by the blank holder force, the interaction between the blank holder force and the blank width, the interaction between the die gap and the blank width, and the interaction between the blank holder force and the die gap, respectively.

Table 13. Analysis of Variance for SN ratios.

Source	DF	Seq SS	Adj SS	Adj MS	F	P	% Contribute
A	2	0.32221	0.32221	0.161103	54.26	0	19.89
B	2	1.03094	1.03094	0.515468	173.63	0	63.65
C	2	0.05408	0.05408	0.02704	9.11	0.009	3.34
AxB	4	0.05174	0.05174	0.012934	4.36	0.037	3.19
AxC	4	0.07071	0.07071	0.017677	5.95	0.016	4.37
BxC	4	0.06635	0.06635	0.016589	5.59	0.019	4.1
Residual Error	8	0.02375	0.02375	0.002969			1.47
Total	26	1.61977					100.01

Table 14. ANOVA of linear regression.

Source	DF	Adj SS	Adj MS	F-Value	P-Value
Regression	3	99.043	33.0143	15.85	0
A	1	14.401	14.4006	6.91	0.015
B	1	84.24	84.2402	40.45	0
C	1	0.402	0.402	0.19	0.665
Error	23	47.901	2.0827		
Total	26	146.944			

3.5. Regression Analysis

Regression analysis [25, 52] is a powerful statistical technique widely used to establish relationships between variables and develop predictive models. It uses a mathematical model for understanding how changes in one or more independent variables influence a dependent variable. In addition, the analyzed equation can also be used as a model for forecasting [53]. Regression analysis has been successfully applied in various engineering and manufacturing applications for process optimization, quality control, and prediction [54-57].

This study uses both linear and quadratic regression analyses to predict the relationship between each variable that was experimentally tested using the Taguchi method that was previously analyzed. Linear regression aims to fit a straight line to the data while quadratic regression allows for a curved relationship providing a more flexible approach for capturing non-linear trends. The data used to create the regression equation will be analyzed using ANOVA from the results of all 27 experimental runs to evaluate the overall fit of the regression models and the importance of individual terms, such as the linear model, the linear model with interaction term, the quadratic model, and the quadratic model with interaction term. The main factors used in the analysis are blank holder force, die gap, and blank width. After performing regression analysis in various forms and finding the best fit values, the predicted results from the model will be compared with those of experiment to confirm the analysis results.

3.5.1. Linear Regression model

In this research, linear regression was used to identify the relationship model. It is a type of multiple linear regression that analyzes only three main factors as independent variables: blank holder force (A), die gap (B), and blank width (C). The analysis using ANOVA found that the regression model is statistically significant, and the factor blank width is not a significant predictor in

the model at a 95% confidence level (P-value > 0.05), as shown in Table 14. Therefore, in order to increase the accuracy and reliability of the model, the term C was removed from the regression model. The residual plot in Fig. 11 displays a normal distribution, a straight line arrangement, and a random pattern of ups and downs around the value of 0. This shows that the model is reliable and usable. The resulting equation from the analysis is shown below.

$$\%Area = 102.62 + 0.0596A - 21.63B \quad (28)$$

R-sq = 67.13%, R-sq (adj) = 64.39%

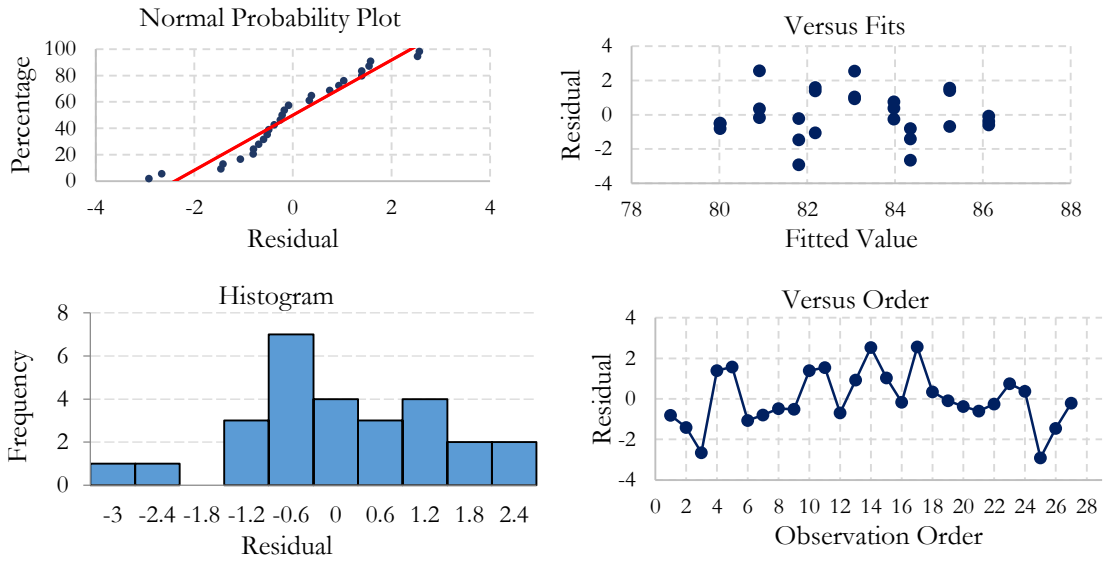

Fig. 11. Residual plot of linear regression.

3.5.2. Linear Regression model with interaction

The second type of regression model adds interaction terms between factors into the equation to study the relationship between each term and the influence of the interaction. From the ANOVA analysis in Table 15, it was found that the regression model was statistically significant, and only terms A and B were significant in the regression model. Meanwhile, other terms were not significant, with P-values > 0.05. Therefore, other terms will not be considered in the model building, leaving only terms A and B, as in the linear regression model mentioned above. This model yields the same result. Therefore, the linear regression with interaction analyzed here will not be used to compare the accuracy and optimize the results of the experiment. The resulting equation from the analysis, and the R-sq and R-sq (adj) values, are shown in the following equation:

$$\%Area = 102.62 + 0.0596A - 21.63B \quad (29)$$

R-sq= 67.13%, R-sq (adj) = 64.39%

Table 15. ANOVA of linear regression with interaction.

Source	DF	Adj SS	Adj MS	F-Value	P-Value
Regression	6	111.848	18.6413	10.62	0
A	1	14.401	14.4006	8.21	0.01
B	1	84.24	84.2402	48.01	0
C	1	0.402	0.402	0.23	0.637
AB	1	3.641	3.641	2.07	0.165
AC	1	3.91	3.9102	2.23	0.151
BC	1	5.254	5.2536	2.99	0.099
Error	20	35.096	1.7548		
Total	26	146.944			

DOI:10.4186/ej.2024.28.10.25

3.5.3. Quadratic regression

Quadratic regression analysis extends beyond linear regression by incorporating a squared term into the equation. Consequently, the model produces a parabolic curve rather than a straight line. This type of regression is used to study curvilinear relationships. The terms added to the equation are A^2, B^2, and C^2. ANOVA analysis in Table 16 shows that the regression model is significant, and all term were significant, except for term C which was not significant with a P-value > 0.05. Therefore, the term C is not included in the quadratic model. Figure 12 shows a quadratic model residual plot that demonstrates that the model features normal data with a linear trend, and the versus plots show a random distribution devoid of any pattern. The resulting equation is as follows:

$$\%Area = 85.527 + 0.744A - 1.8B - 1.097A^2 - 0.843\,B^2 - 0.607C^2 \quad (30)$$

R-sq = 86.57%, R-sq (adj) = 83.37%.

Table 16. ANOVA of quadratic regression.

Source	DF	Adj SS	Adj MS	F-Value	P-Value
Regression	6	127.609	21.2681	22	0
A	1	14.401	14.4006	14.9	0.001
B	1	84.24	84.2402	87.14	0
C	1	0.402	0.402	0.42	0.526
A^2	1	15.063	15.0628	15.58	0.001
B^2	1	8.898	8.8979	9.2	0.007
C^2	1	4.605	4.6054	4.76	0.041
Error	20	19.335	0.9668		
Total	26	146.944			

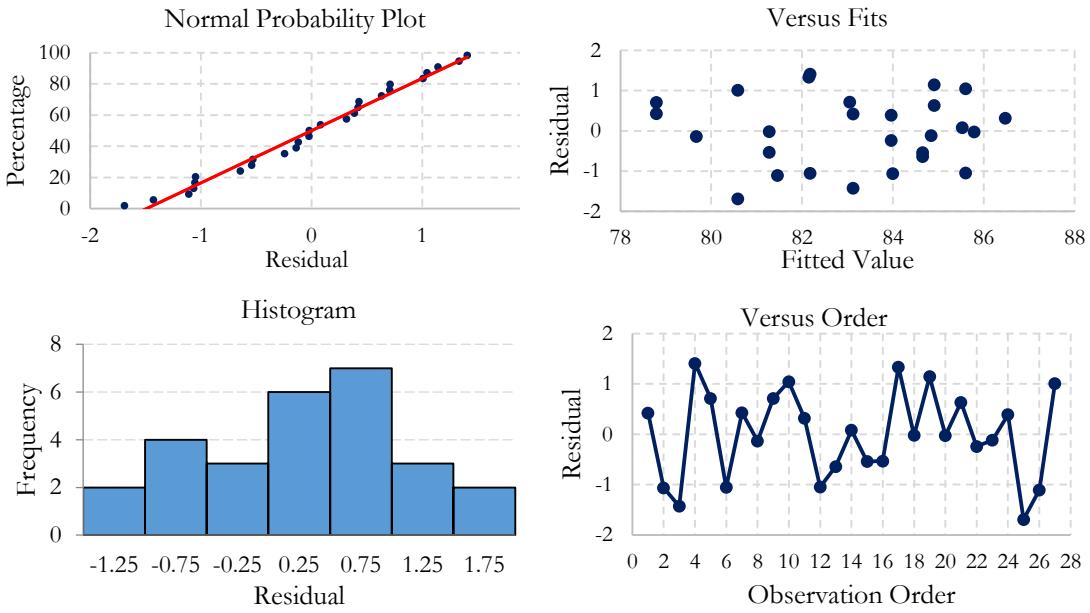

Fig. 12. Residual plot of quadratic regression.

3.5.4. Quadratic regression with interaction

The final regression analysis is a quadratic analysis that adds an interaction term between the variables to fully capture the second-order and interaction effects. An Analysis of Variance (ANOVA) from Table 17 shows that the model was statistically significant, while only term C was not significant. Therefore, term C was removed from the model analysis. Figure 13 shows the residual plot of the quadratic regression fit with interaction terms. The data were found to be normally distributed and clustered around a straight line. The versus plot showed that the data were randomly distributed with no fixed pattern and scattered around the value of 0, indicating the reliability of the model without experimental design. The resulting quadratic regression equation with interaction is as follows:

$$\begin{aligned} \%Area = {} & 85.527 + 0.744A - 1.800B \\ & - 1.097A^2 - 0.843B^2 \\ & - 0.607C^2 - 0.381AB \\ & + 0.395AC + 0.458BC \end{aligned} \quad (31)$$

R-sq = 95.28%, R-sq (adj) = 93.19%

Table 17. ANOVA of quadratic regression with interaction.

Source	DF	Adj SS	Adj MS	F-Value	P-Value
Regression	9	140.414	15.6015	40.62	0
A	1	14.401	14.4006	37.49	0
B	1	84.24	84.2402	219.3	0
C	1	0.402	0.402	1.05	0.321
A^2	1	15.063	15.0628	39.21	0
B^2	1	8.898	8.8979	23.16	0
C^2	1	4.605	4.6054	11.99	0.003
AB	1	3.641	3.641	9.48	0.007
AC	1	3.91	3.9102	10.18	0.005
BC	1	5.254	5.2536	13.68	0.002
Error	17	6.53	0.3841		
Total	26	146.944			

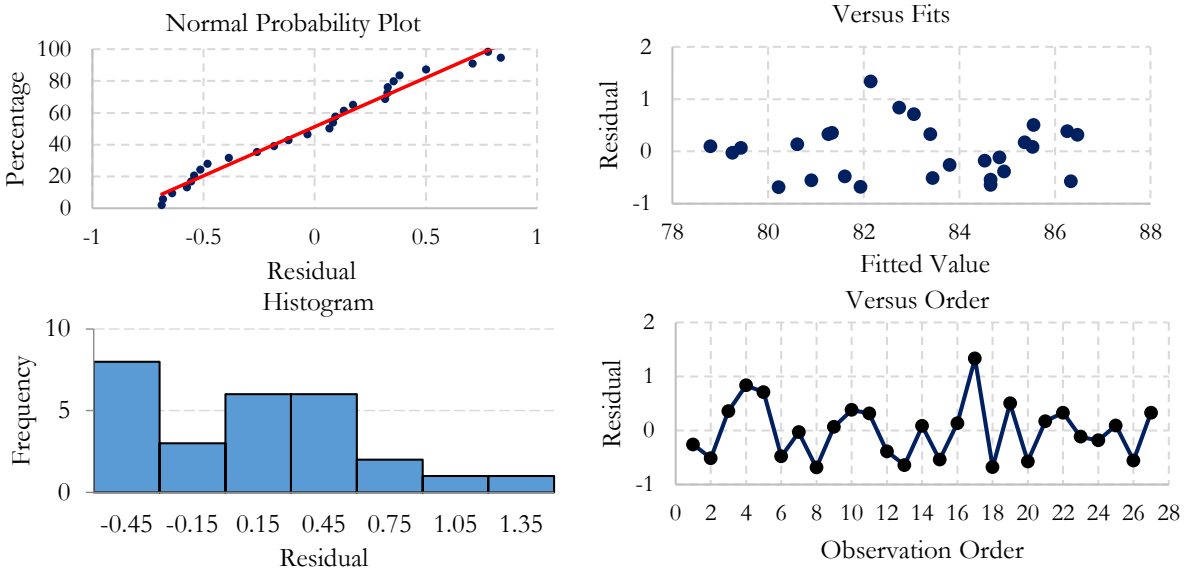

Fig. 13. Residual plot of quadratic regression with interaction.

The analysis of various regression models revealed that the quadratic regression model with interaction, with values of 95.56% and 93.2%, had the highest R-sq and R-sq (adj) values, indicating that the predicted values were closest to the experimental values. Therefore, this model was selected in this regression analysis to optimize the process parameters to maximize the percentage of area in the displacement range of -1 to 1 mm.

3.6. Optimization with Desirability Function Analysis and Confirmation

After selecting the regression model to be used for optimization to find the variable values that minimize workpiece distortion, or in this case, maximize the percentage of area of displacement between the simulated and reference parts in the range of -1 to 1 mm, the results of the regression analysis were optimized using the desirability function analysis proposed by Derringer and Suich in 1980 [57]. This method transforms the response variable values into desirability values, which range from 0 to 1. The value of a response increases as the response value approaches the target value. When it is 0, it indicates that the response value is unacceptable. When it is 1, it indicates that the response value has reached the desired target. There are three types of equations for calculating desirability: the nominal-the-better, the smaller-the-better, and the larger-the-better. In this work, we aim to maximize the percentage of area within a specific dimensional range (-1 to 1 mm). Therefore, a larger-the-better type objective function is employed. Consequently, the target value for optimization is set to the maximum achievable percentage within this range. The desirability function equation for the larger-the-better type is shown below [57]:

$$d_i = \begin{cases} 0 & y_i \le y_{min} \\ \left(\dfrac{y_i - y_{min}}{y_{max} - y_{min}}\right)^r & y_{min} \le y_i \le y_{max}, \\ 1 & r \ge 0 \\ & y_i \ge y_{min} \end{cases} \quad (32)$$

where d_i is the response obtained from the i-th experiment, y_{min} is the lower tolerance limit response that is acceptable, y_{max} is the upper tolerance limit response that is acceptable, and r is the weight value or shape of the desirability function. Here, it can be replaced by 0.1, 1, and 10 according to the form of the function. The value of d_i in each experiment is combined from multiple d_i values to form a global desirability (d_g) according to the following equation:

$$d_G = \sqrt[w]{({d_1}^{w_1} x {d_2}^{w_2} x {d_3}^{w_3} \ldots . x {d_i}^{w_i})} \quad (33)$$

where d_i is the individual desirability of each response, w_i is the weight of each response, and w is the sum of all weights. The values used for optimization in the experiment are shown in Table 18. The results of the optimization are shown in Fig. 14. The optimization results showed that the process parameters obtained from the optimization using quadratic regression with interaction were as follows: blank holder force = 41.21 tons, die gap = 0.9 mm, and blank width = 297.47 mm. The response value, or percentage of area, was 86.85% with a maximum d-value of 1. This can indicate the highest predicted percentage of area within the -1 to 1 mm displacement range. From this chart, when decreasing or increasing blank holder force or blank width, it leads to a decrease in the desirability function. This effect represents the lower percentage of area than the optimal point. Similarly, increasing the die gap causes the percentage of area to decrease. When comparing the optimization results with the experimental results shown in Table 19, which used the same parameters, the response values obtained from the prediction and experiment were close, at 86.85 % and 86.81%, respectively.

Table 18. Optimization condition.

Response	Goal	Lower	Target	Upper	Weight
%Area	Maximize	78.89	86.79	86.79	10

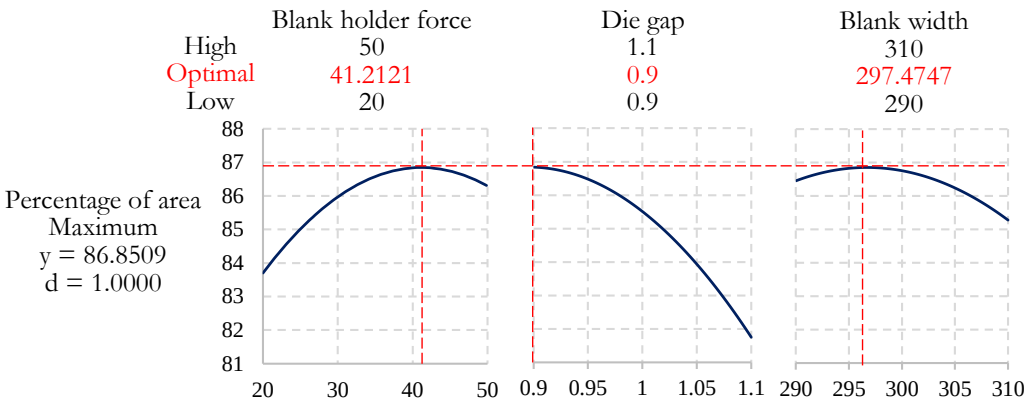

Fig. 14. Optimization result by using quadratic model with interaction.

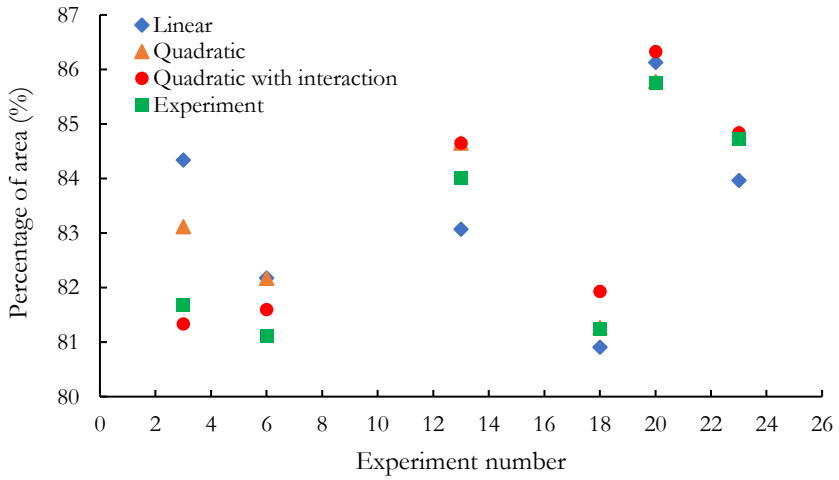

Fig. 15. Prediction result comparison and confirmation.

Table 19. Optimization result confirmation.

Response	Optimal parameter			Predict (%)	Experiment (%)
	Blank holder force (ton)	Die gap (mm)	Blank width (mm)		
Percentage of area	41.21	0.9	297.47	86.85	86.81

3.7. Regression Model Comparison

The predicted results from each regression model were compared with the experimental results to confirm the accuracy and compare the precision of the predicted results from different models. All 6 sets of process parameters were randomly sampled from the experimental results obtained in the Taguchi L27 orthogonal design experiment. The comparison results showed that the predicted results from all models, as presented in Figure 15, were close to the experimental results, and it was found that the predicted results from the quadratic model were closer to the actual experimental results than those from the linear model.

4. Conclusion

This research compared material models used in FEM simulation to select the most accurate model. The Taguchi method was applied to analyze the relevant variables and investigate their influence. The orthogonal array L_{27} (3^3) was selected to study the influence of all factors and interactions between variables. An ANOVA was used to confirm the experiment and the influence of various factors at a 95% confidence level. After the analysis, the optimal value was found by using the average value and comparing it with the experimental results. The data were then analyzed and fitted with various regression models. An ANOVA was used to determine which variables were statistically significant and whether the

model was reliable at a 95% confidence level. The following models were analyzed:

- Linear regression model
- Linear regression model with interaction
- Quadratic regression model
- Quadratic regression model with interaction

The R-square and R-square (adj) values were compared. The model with the highest reliability was used for optimization to find the process parameters that maximize the percentage of area in the displacement range between the desired workpiece shape and the simulated workpiece shape. The optimized results were confirmed with experimental results. Finally, the accuracy of the predicted results from all regression models was compared to determine the most accurate model. The experimental results can be summarized as follows:

- The material model using the Y-U hardening model is more accurate than the pure isotropic hardening model.
- The most accurate material model for FEM simulation is the Barlat 1989 combined with the Y-U model.
- The optimal process parameters obtained from the Taguchi S/N ratio analysis (larger the better) are blank holder force = 35 tons, die gap = 0.9 mm, and blank width = 300 mm.
- The predicted response value from the Taguchi analysis using the optimal parameters considering the interaction between variables is 86.9%, which is close to the experimental response value.
- An ANOVA analysis of the Taguchi experiment revealed that the most influential variable is the die gap, followed by the blank holder force, the interaction between the blank holder force and the blank width, the interaction between the die gap and the blank width, and the interaction between the blank holder force and the die gap. The percentage contributions are 63.65%, 19.89%, 4.37%, 4.1%, 3.34%, and 3.19%, respectively.
- In the construction of regression models with different equation forms, the linear regression with interaction was not considered because the blank width and all interaction terms were not significant predictor terms in the ANOVA analysis. All models are reliable at a 95% confidence level. The quadratic regression model with interaction was selected to optimize the process parameters. This model gives the highest R-square and R-square (adj) values of 95.28% and 93.19%, respectively.
- The optimal parameters for maximizing the response predicted by the quadratic regression model with interaction using the desirability function analysis are: blank holder force = 41.21 tons, die gap = 0.9 mm, and blank width = 297.47 mm. The predicted response value is 86.85%, which is very accurate compared to the experimental result with the same parameters, with a difference of only 0.04%.

The predicted results of various regression models were compared with the experimental results of 6 randomly selected experiments from the Taguchi L_{27} (3^3) design. The quadratic regression model was found to be the most accurate model, with predicted values close to the experimental results.

Acknowledgement

The authors gratefully acknowledge the financial support from the National Research Council of Thailand (NRCT) under the Research and Researcher for Industries (RRI) Grant No. 61I0053. We would also like to express our sincere appreciation to Thai Summit Automotive Co., Ltd. for their contribution of experimental materials, specimens, and testing equipment. Their support was instrumental in the completion of this research.

References

[1] M. Lai and R. Brun, "Latest developments in sheet metal forming technologies and materials for automotive application: The use of ultra high strength steels at fiat to reach weight reduction at sustainable costs," *Key Eng Mater*, vol. 344, pp. 1-8, Jul. 2007.

[2] K. Lange and K. Pöhlandt, *Handbook of Metal Forming*. Society of Manufacturing Engineers, 1994.

[3] S. Kalpakjian and S. Schmid, *Manufacturing Engineering & Technology*, 7th ed. Pearson, 2013.

[4] W. Gan and R. H. Wagoner, "Die design method for sheet springback," *Int J Mech Sci*, vol. 46, no. 7, pp. 1097-1113, Jul. 2004.

[5] H. Yang, J. Chen, Q. Hong, and W. Chen, "Development of combined hardening model for spring-back simulation of DP600 in multi-stage sheet metal forming," *Journal of Physics: Conference Series*, Institute of Physics, vol. 2585, no. 1, p. 012008, 2023.

[6] A. D. Anggono, W. A. Siswanto, and B. Omar, "Algorithm development and application of spring back compensation for sheet metal forming," *Research Journal of Applied Sciences, Engineering and Technology*, vol. 4, no. 14, pp. 2036-2045, 2012.

[7] R. Lingbeek, J. Huétink, S. Ohnimus, M. Petzoldt, and J. Weiher, "The development of a finite elements based springback compensation tool for sheet metal products," *J Mater Process Technol*, vol. 169, no. 1, pp. 115-125, Oct. 2005.

[8] S. Thipprakmas and W. Phanitwong, "Process parameter design of spring-back and spring-go in V-bending process using Taguchi technique," *Mater Des*, vol. 32, no. 8-9, pp. 4430-4436, Sep. 2011.

[9] M. özdemir, "Optimization of spring back in air V bending processing using Taguchi and RSM Method," *Mechanics*, vol. 26, no. 1, pp. 73-81, Feb. 2020.

[10] J. Duraisamy, S. Saravanan, M. Saravanan, and D. Jeyasimman, "Experimental prediction and investigation of spring back in u bending profile process using RSM and ANOVA," *International Journal of Mechanical and Production Engineering Research and Development,* vol.9, pp. 760-772, Jun. 2019.

[11] G. Ingarao, R. Di Lorenzo, and F. Micari, "Analysis of stamping performances of dual phase steels: A multi-objective approach to reduce springback and thinning failure," *Mater Des*, vol. 30, no. 10, pp. 4421-4433, Dec. 2009.

[12] N. Panda and R. S. Pawar, "Optimization of process parameters affecting on spring-back in V-bending process for high strength low alloy steel HSLA 420 using FEA (HyperForm) and Taguchi Technique." *International Journal of Aerospace and Mechanical Engineering,* vol.12, no.1, pp. 28-34, 2018.

[13] H. Zein, M. El Sherbiny, M. Abd-Rabou, and M. El shazly, "Thinning and spring back prediction of sheet metal in the deep drawing process," *Mater Des*, vol. 53, pp. 797-808, 2014.

[14] W. Julsri, S. Suranuntchai, and V. Uthaisangsuk, "Finite element based analysis of two-stage forming for advanced high strength steel part," *Procedia Manufacturing*, vol. 15, pp. 668-675, 2018.

[15] K. Lawanwong, H. Hamasaki, R. Hino, and F. Yoshida, "Double-action bending for eliminating springback in hat-shaped bending of advanced high-strength steel sheet," *International Journal of Advanced Manufacturing Technology*, vol. 106, no. 5-6, pp. 1855-1867, Jan. 2020.

[16] S. Konzack, R. Radonjic, M. Liewald, and T. Altan, "Prediction and reduction of springback in 3D hat shape forming of AHSS," *Procedia Manufacturing*, vol. 15, pp. 660-667, 2018.

[17] K. Chen, J. P. Lin, M. K. Lv, and L. Y. Wang, "Advanced high strength steel sheet forming and springback simulation," *Adv Mat Res*, vol. 97-101, pp. 200-203, Mar. 2010.

[18] V. C. Tong and D. T. Nguyen, "A study on spring-back in U-draw bending of DP350 high-strength steel sheets based on combined isotropic and kinematic hardening laws," *Advances in Mechanical Engineering*, vol. 10, no. 9, Sep. 2018.

[19] B. Chongthairungruang, V. Uthaisangsuk, S. Suranuntchai, and S. Jirathearanat, "Springback prediction in sheet metal forming of high strength steels," *Mater Des*, vol. 50, pp. 253-266, 2013.

[20] H. U. Hassan, H. Traphöner, A. Güner, and A. E. Tekkaya, "Accurate springback prediction in deep drawing using pre-strain based multiple cyclic stress-strain curves in finite element simulation," *Int J Mech Sci*, vol. 110, pp. 229-241, May. 2016.

[21] R. Narayanasamy and P. Padmanabhan, "Modeling of springback on air bending process of interstitial free steel sheet using multiple regression analysis," *International Journal on Interactive Design and Manufacturing (IJIDeM)*, vol. 3, pp. 25-33, 2009.

[22] M. S. Buang, S. A. Abdullah and J. Saedon, "Optimization of springback prediction in U-channel process using response surface methodology," *International Journal of Mechanical and Mechatronics Engineering*, vol. 9, no. 7, pp. 1216-1223, 2015.

[23] E. Ferreira, A. Maia, M. C. Oliveira, L. F. Menezes, and A. Andrade-Campos, "Optimization strategies and statistical analysis for springback compensation in sheet metal forming," in *COMPLAS XIII: International Conference on Computational Plasticity*, Barcelona, Spain, 2015, pp. 759-770.

[24] D. C. Montgomery, E. A. Peck, and G. G. Vining, "Introduction to linear regression analysis," in *Introduction to Linear Regression Analysis*, 6th ed. Hoboken, NJ: Wiley, 2021.

[25] N. R. Draper and H. Smith, *Applied Regression Analysis*. John Wiley & Sons, 1998, vol. 326.

[26] F. Yoshida and T. Uemori, "A model of large-strain cyclic plasticity describing the Bauschinger effect and workhardening stagnation," *International Journal of Plasticity*, vol. 18, pp. 661-686, Oct. 2002.

[27] W. Julsri, S. Suranuntchai, and V. Uthaisangsuk, "Study of springback effect of AHS steels using a microstructure based modeling," *Int J Mech Sci*, vol. 135, pp. 499-516, Jan. 2018.

[28] R. Hill, "A theory of the yielding and plastic flow of anisotropic metals," in *Proceedings of the Royal Society of London. Series A. Mathematical and Physical Sciences,* 1948, pp. 281-297.

[29] H. Hencky, "On a theory of plastic deformations and the corresponding stresses," *Journal of Applied Mathematics and Mechanics/Zeitschrift für Angewandte Mathematik und Mechanik*, vol. 4, pp. 323-334, 1924.

[30] F. Barlat and O. Richmond, "Prediction of tricomponent plane stress yield surfaces and associated flow and failure behavior of strongly textured F.C.C. polycrystalline sheets," *Materials Science and Engineering*, vol. 95, pp. 15-29, Nov. 1987.

[31] W. F. Hosford, "On yield loci of anisotropic cubic metals," in *Proceedings of the Seventh North American Metal working Conference SME*, 1979, pp. 191-197.

[32] S. Panich, M. Liewald, and V. Uthaisangsuk, "Stress and strain based fracture forming limit curves for advanced high strength steel sheet," *Int. J. Mater. Form.*, vol. 11, pp. 643-661, 2018.

[33] V. Panahizadeh, Y. D. Asl, F. Saeedi, and S. Afshin, "Anisotropic analysis of springback in FRF process with variable cross section using Hill and Barlat criteria," 2021.

[34] B. Tang, X. Lu, Z. Wang, and Z. Zhao, "Springback investigation of anisotropic aluminum alloy sheet with a mixed hardening rule and Barlat yield criteria

in sheet metal forming," *Mater. Des.*, vol. 31, no. 4, pp. 2043-2050, 2010.
[35] S. Toros, A. Polat, and F. Ozturk, "Formability and springback characterization of TRIP800 advanced high strength steel," *Mater. Des.*, vol. 41, pp. 298-305, 2012.
[36] D. Koreček, P. Solfronk, and J. Sobotka, "Analysis of TRIP steel HCT690 deformation behaviour for prediction of the deformation process and spring-back of the material via numerical simulation," *Materials*, vol. 17, no. 3, Feb. 2024
[37] J. L. Chaboche and G. Rousselier, "On the plastic and viscoplastic constitutive equations—Part I: Rules developed with internal variable concept," *J. Pressure Vessel Technol.*, vol. 105, no. 2, pp. 153-158, 1983.
[38] F. Yoshida, T. Uemori, and K. Fujiwara, "Elastic-plastic behavior of steel sheets under in-plane cyclic tension-compression at large strain," *International Journal of Plasticity*, vol. 18, pp. 633-659, Oct. 2002.
[39] A. Sanrutsadakorn, N. Jhonthong, and W. Julsri, "Finite element modeling for analyzing the production of high-strength steel sheets for automobile parts," *Materials Research Express*, vol. 11, p. 106524, 2024.
[40] A. Sunanta and S. Suranuntchai, "Comparative study on some appropriate material models for automotive ultra-high strength steels parts using FE simulation," in *Proc. 2020 IEEE 7th Int. Conf. Ind. Eng. Appl. (ICIEA)*, pp. 211-215, Apr. 2020.
[41] B. Chongthairungruang, V. Uthaisangsuk, S. Suranuntchai, and S. Jirathearanat, "Experimental and numerical investigation of springback effect for advanced high strength dual phase steel," *Mater. Des.*, vol. 39, pp. 318-328, 2012.
[42] Y. Zhang, L. Lang, Y. Wang, H. Chen, J. Du, Z. Jiao, and L. Wang, "Spring back behavior of large multi-feature thin-walled part in rigid-flexible sequential loading forming process," *Materials*, vol. 15, no. 7, p. 2608, 2022.
[43] ESI Group, *PAM-STAMP 2022 User Guide*. 2022.
[44] P. J. Ross, *Taguchi Techniques for Quality Engineering: Loss Function, Orthogonal Experiments, Parameter and Tolerance Design*. New York: McGraw-Hill, 1996.
[45] M. S. Phadke, *Quality Engineering Using Robust Design*. Prentice Hall PTR, 1995.
[46] G. Taguchi, S. Chowdhury, and Y. Wu, *Taguchi's Quality Engineering Handbook*. 2004.
[47] O. Köksoy and F. Zehra Muluk, "Solution to the Taguchi's problem with correlated responses," *Gazi University Journal of Science*, vol. 17, no. 1, pp. 59-70, 2004.
[48] G. Taguchi, "Robust technology development," *Mechanical Engineering-CIME*, vol. 115, no. 3, pp. 60-63, 1993.
[49] G. Taguchi, "System of experimental design; engineering methods to optimize quality and minimize costs," in *Quality Resources*, 1st ed., 1987.
[50] R. K. Roy, *A primer on the Taguchi method*. Society of Manufacturing Engineers, 2010.
[51] R. G. Miller Jr, *Beyond ANOVA: Basics of Applied Statistics*. CRC press, 1997.
[52] T. P. Ryan, *Modern Regression Methods*. John Wiley & Sons, 2008, vol. 655.
[53] D. G. Kleinbaum, L. L. Kupper, A. Nizam, and K. E. Muller, *Applied Regression Analysis and Other Multivariable Methods*, 5th ed. Boston, MA, USA: Cengage Learning, 2013.
[54] T. Jantarasricha, "Assessment of the relationship between lubricating oil viscosity and surface-attached adhesion rate via regression modelling," *J. Eng. Appl. Sci.*, vol. 70, no. 1, p. 94, 2023.
[55] A. E. Marques, P. A. Prates, A. F. Pereira, M. C. Oliveira, J. V. Fernandes, and B. M. Ribeiro, "Performance comparison of parametric and non-parametric regression models for uncertainty analysis of sheet metal forming processes," *Metals*, vol. 10, no. 4, p. 457, 2020.
[56] T. Trzepieciński, M. Szpunar, and Ľ. Kaščák, "Modeling of friction phenomena of Ti-6Al-4V sheets based on backward elimination regression and multi-layer artificial neural networks," *Materials*, vol. 14, no. 10, p. 2570, 2021.
[57] M. Murugesan, J.-H. Yu, K.-S. Jung, S.-M. Cho, K. S. Bhandari, and C.-W. Lee, "Optimization of forming parameters in incremental sheet forming of AA3003-H18 sheets using Taguchi method," *Materials*, vol. 15, no. 4, p. 1458, 2022.
[58] G. Derringer and R. Suich, "Simultaneous optimization of several response variables," *Journal of Quality Technology*, vol. 12, no. 4, pp. 214-219, 1980.

Aekkapon Sunanta, photograph and biography not available at the time of publication.

Weerapong Julsri, photograph and biography not available at the time of publication.

Surasak Suranuntchai, photograph and biography not available at the time of publication.